energies

MDPI

Article

Spectacular Enhancement of the Thermal and Photochemical Stability of $MAPbI_3$ Perovskite Films Using Functionalized Tetraazaadamantane as a Molecular Modifier

Victoria V. Ozerova [1,2], Ivan S. Zhidkov [3,4], Aleksandra Boldyreva [5], Nadezhda N. Dremova [1], Nikita A. Emelianov [1], Gennady V. Shilov [1], Lyubov A. Frolova [1], Ernst Z. Kurmaev [3,4], Alexey Y. Sukhorukov [6,7], Sergey M. Aldoshin [1] and Pavel A. Troshin [1,*]

1 The Institute for Problems of Chemical Physics of the Russian Academy of Sciences (IPCP RAS), Semenov Prospect 1, 141432 Chernogolovka, Russia; podsolnuz@gmail.com (V.V.O.); dremova@icp.ac.ru (N.N.D.); emelianov@icp.ac.ru (N.A.E.); genshil@icp.ac.ru (G.V.S.); lyubovanatolievna@mail.ru (L.A.F.); sma@icp.ac.ru (S.M.A.)
2 Higher Chemical College of Russian Academy of Sciences, D. Mendeleev University of Chemical Technology of Russia, Miusskaya sq. 9, 125947 Moscow, Russia
3 Institute of Physics and Technology, Ural Federal University, Mira st. 19, 620002 Yekaterinburg, Russia; i.s.zhidkov@urfu.ru (I.S.Z.); ernst.kurmaev@gmail.com (E.Z.K.)
4 M. N. Mikheev Institute of Metal Physics of Ural Branch of Russian Academy of Sciences, S. Kovalevskoi st. 18, 620108 Yekaterinburg, Russia
5 Skolkovo Institute of Science and Technology, Bolshoy Boulevard 30, bld. 1, 121205 Moscow, Russia; aleksandra.boldyreva@skolkovotech.ru
6 N. D. Zelinsky Institute of Organic Chemistry of Russian Academy of Sciences, Leninsky Prospect, 47, 119991 Moscow, Russia; a.yu.sukhorukov@gmail.com
7 Plekhanov Russian University of Economics, 117997, Stremyanny Per. 36, 115093 Moscow, Russia
* Correspondence: troshin2003@inbox.ru

Abstract: Perovskite solar cells represent a highly promising third-generation photovoltaic technology. However, their practical implementation is hindered by low device operational stability, mostly related to facile degradation of the absorber materials under exposure to light and elevated temperatures. Improving the intrinsic stability of complex lead halides is a big scientific challenge, which might be addressed using various "molecular modifiers". These modifiers are usually represented by some additives undergoing strong interactions with the perovskite absorber material, resulting in enhanced solar cell efficiency and/or operational stability. Herein, we present a derivative of 1,4,6,10-tetraazaadamantane, **NAdCl**, as a promising molecular modifier for lead halide perovskites. **NAdCl** spectacularly improved both the thermal and photochemical stability of methylammonium lead iodide ($MAPbI_3$) films and, most importantly, prevented the formation of metallic lead Pb^0 as a photolysis product. **NAdCl** improves the electronic quality of perovskite films by healing the traps for charge carriers. Furthermore, it strongly interacts with the perovskite framework and most likely stabilizes undercoordinated Pb^{2+} ions, which are responsible for Pb^0 formation under light exposure. The obtained results feature 1,4,6,10-tetraazaadamantane derivatives as highly promising molecular modifiers that might help to improve the operational lifetime of perovskite solar cells and facilitate the practical implementation of this photovoltaic technology.

Keywords: perovskite solar cells; complex lead halides; photostability; thermal stability; molecular additives; molecular modifiers

Citation: Ozerova, V.V; Zhidkov, I.S; Boldyreva, A.; Dremova, N.N; Emelianov, N.A; Shilov, G.V; Frolova, L.A; Kurmaev, E.Z; Sukhorukov, A.Y; Aldoshin, S.M; et al. Spectacular Enhancement of the Thermal and Photochemical Stability of $MAPbI_3$ Perovskite Films Using Functionalized Tetraazaadamantane as a Molecular Modifier. *Energies* **2021**, *14*, 669. https://doi.org/10.3390/en14030669

Received: 30 December 2020
Accepted: 25 January 2021
Published: 28 January 2021

1. Introduction

Perovskite solar cells have recently attracted tremendous attention among academic and industry research communities due to their impressive efficiency records, surpassing 25.5% and coming close to the performance of the best laboratory samples of crystalline silicon solar cells [1]. Some efforts have been made to commercialize perovskite photovoltaics,

particularly using high-efficiency monolithic perovskite–silicon tandem devices [2]. Unfortunately, the commercial potential of this technology is severely restricted by the low operational stability of perovskite solar cells [3]. The stability issues are related, in particular, to facile degradation of perovskite-type absorber materials induced by ambient species (moisture, oxygen, CO_2) [4–8], as well as elevated temperatures [9–11] and light [12–14].

Several molecular and supramolecular chemistry approaches were developed in order to overcome the low intrinsic stability of complex lead halides [15–21]. In particular, the ambient stability of perovskite films can be boosted by coating them with thin layers of strongly hydrophobic reagents comprising long alkyl chains and/or aromatic fragments, often loaded with fluorine substituents, which are known to be moisture-repellent [22–25]. Furthermore, the truly 3D perovskite structure can be converted to a large variety of 2D or 2D/3D architectures by introducing additional amounts of ammonium salts, usually with bulky organic cations [26–28]. It has been reported in a number of studies that decreasing the dimensionality of the perovskite lattice improves the ambient stability of the absorber materials, as well as the operational stability of perovskite solar cells [29–31].

Using adamantane and, especially, adamantylammonium salts as reagents to modify perovskite films has delivered quite impressive results. In particular, loading perovskite films with either pristine adamantane or 1-adamantylamine resulted in passivation of the surface defects at the grain boundaries and improvements in the solar cell open-circuit voltage (V_{OC}) and power conversion efficiency (PCE) [32]. This modification also substantially increased the hydrophobicity of perovskite films and improved their ambient stability. Furthermore, perovskite solar cells comprising adamantane and, in particular, adamantylamine showed enhanced operational stability under 1-sun illumination as compared to reference cells based on non-modified perovskite.

The incorporation of adamantylammonium salts in the hole-transport layer of 2,2′,7,7′-tetrakis[N,N-di(4-methoxyphenyl)amino]-9,9′-spirobifluorene (spiro-OMeTAD) was reported to improve the interface with the perovskite absorber, thus resulting in enhanced device V_{OC} and PCE [33]. Passivation of the interfacial trap states also boosted the operational stability of perovskite solar cells: virtually no decay in the efficiency was observed within 500 h under 1-sun illumination for devices incorporating adamantylammonium iodide, whereas the reference cells showed considerable degradation under the same conditions. Adamantylammonium chloride in combination with formamidinium chloride was applied as a molecular modulator to control the perovskite crystallization, leading to improved device performance and stability [34].

Adamantylammonium and adamantylmethylammonium iodides were also used as building blocks to design layered 2D Ruddlesden–Popper perovskite-like phases, which were thoroughly investigated using a series of complementary techniques [35]. The optimal $A_2FA_2Pb_3I_{10}$ (FA–formamidinium cation) material formulations delivered efficiencies exceeding 7% in mesoscopic device architectures without any additional treatment or use of antisolvents, which was an important improvement compared to other reported state-of-the-art FA-based 2D perovskites. The designed 2D absorber materials exhibited good operational stability and excellent resistance to moisture due to the presence of bulky hydrophobic adamantane fragments in their structure. Adamantylammonium salts were also used as passivation reagents for perovskite quantum dots, leading to enhanced luminescence and improved stability [36].

The presented literature overview clearly shows that adamantane and its functional derivatives represent a promising family of molecular modifiers that can be used to control the structure and properties of perovskite films. While the positive effect of such modification on the ambient and operational stability of perovskite solar cells is well documented, the impact of adamantane derivatives on the intrinsic thermal and photochemical stability of the absorber films has not been studied so far. Furthermore, among the vast diversity of known nitrogen-substituted aza-analogs of adamantane, only 1,3,5,7-tetraazaadamantane or urotropin was investigated as a reagent to passivate defects at the grain boundaries in perovskite films [37].

Herein, we explored for the first time 4,6,10-trihydroxy-1,4,6,10-tetraazaadamantane hydrochloride (**NAdCl**) as a molecular modifier for methylammonium lead iodide ($MAPbI_3$) perovskite films. We show that this reagent passivates trap states in $MAPbI_3$, improves the electronic quality of this material, and spectacularly enhances the intrinsic photochemical and thermal stability of the perovskite films.

2. Results

The presence of multiple nitrogen atoms capable of coordinating lead cations in aza-derivatives of adamantane makes them highly promising molecular modifies for perovskite absorber films. In this work, we investigated **NAdCl**, which was synthesized from readily available chloroacetone (Scheme 1) using a modified two-step literature method [38]. The details on the synthesis and spectroscopic characterization of this material are provided in Section 4 below. It is worth mentioning that **NAdCl** represents just an individual exemplary compound from a large family of relevant azaadamantane derivatives that were previously used to design water-soluble phthalocyanines [39], boronate-based covalent organic frameworks [40], and high-valence manganese complexes with interesting magnetic properties [41], among other things.

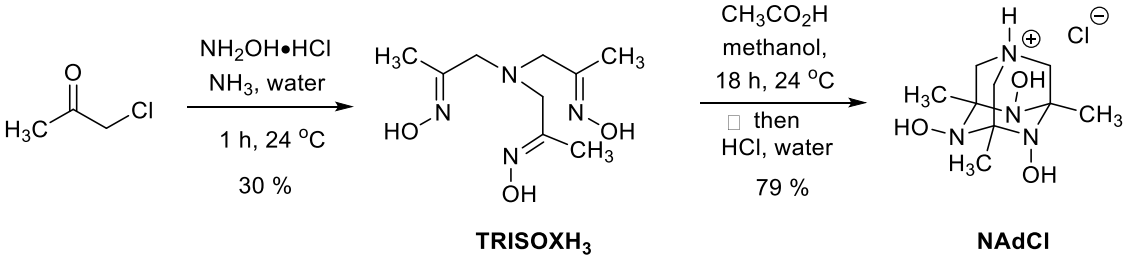

Scheme 1. Synthesis of **NAdCl** from chloroacetone.

It should be emphasized that **NAdCl** also comprises three hydroxyl groups in its structure, which might enable additional supramolecular interactions such as hydrogen bonding [38] or N–O–M covalent bond formation [41]. Since **NAdCl** represents an ammonium salt, we incorporated it in $MAPbI_3$ perovskite precursor solution to obtain the quasi-2D perovskite formulation $NAd_2MA_{39}Pb_{40}I_{119}Cl_2$, following previous reports where other AX ammonium salts were used to design "$A_2MA_{39}Pb_{40}X_{121}$" frameworks in a straightforward manner [42–44]. While it is often assumed that $A_2MA_{39}Pb_{40}X_{121}$ compounds have a homogeneous distribution of A cations within the crystal structure, there are multiple indications of the accumulation of bulky A^+ cations mostly on the surface of the perovskite grains and at the grain boundaries, thus providing the desired grain covering coupled with the passivation of defects [45]. Therefore, we consider **NAdCl**, used in this work, as a molecular modifier of the perovskite films, leaving beyond the scope of the discussion the structural aspects of this modification.

Following our standard approach, the reference $MAPbI_3$ and $NAd_2MA_{39}Pb_{40}I_{119}Cl_2$ films (thickness 450–500 nm) were prepared by spin coating inside a nitrogen-filled glove box. Scanning electron microscopy (SEM) and atomic force microscopy (AFM) showed that the introduction of **NAdCl** drastically changed the film morphology. The $MAPbI_3$ films had a typical morphology with distinct and rather large grains (200–600 nm) with well-defined grain boundaries (Figure 1a,c). On the contrary, $NAd_2MA_{39}Pb_{40}I_{119}Cl_2$ films were composed mostly of tiny fused grains (<20 nm) and had some pores that appeared presumably due to the evaporation of the solvent (DMF) strongly interacting with **NAdCl**, e.g., via hydrogen bonding. Furthermore, the $NAd_2MA_{39}Pb_{40}I_{119}Cl_2$ films were considerably smoother than the $MAPbI_3$ reference films, as concluded from the AFM topography images. The obtained results demonstrate the effect of compositional engineering on the structure of the absorber material films.

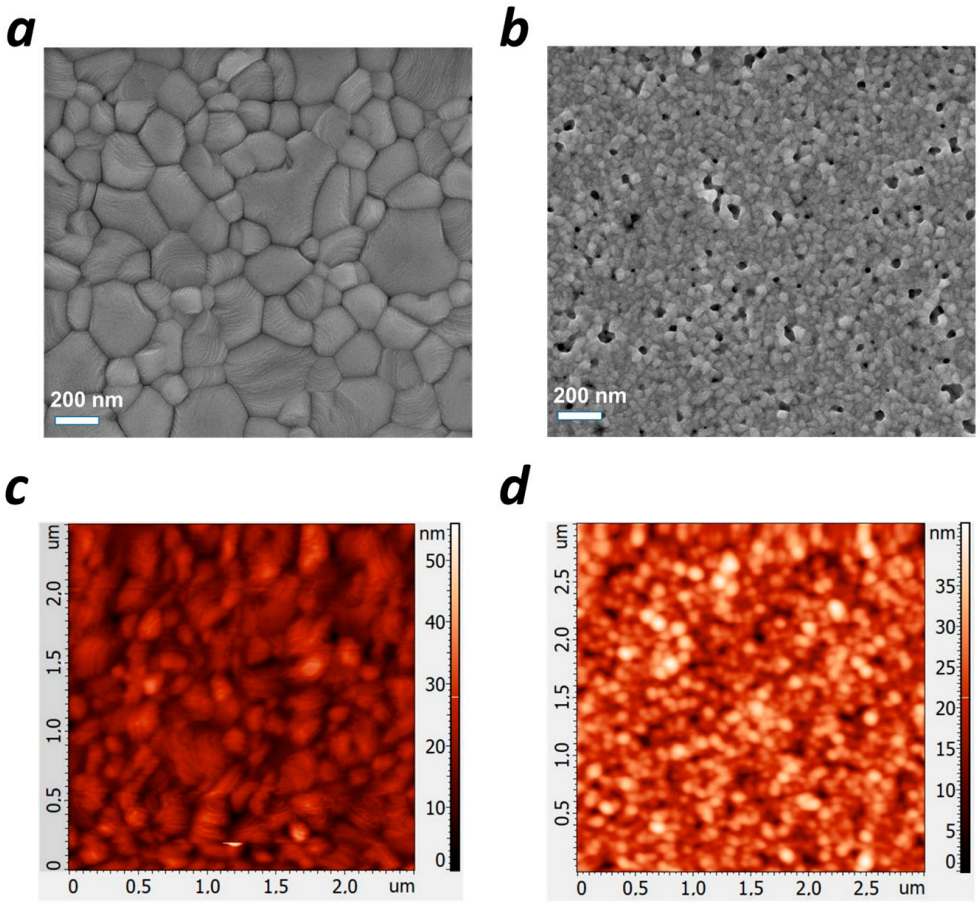

Figure 1. (**a**,**b**) SEM and (**c**,**d**) AFM images of (**a**,**c**) $MAPbI_3$ and (**b**,**d**) $NAd_2MA_{39}Pb_{40}I_{119}Cl_2$ films.

The spin-coated $MAPbI_3$ and $NAd_2MA_{39}Pb_{40}I_{119}Cl_2$ films were transferred to another glove box with integrated aging setups without any contact with ambient oxygen and moisture. The samples were subjected to continuous light soaking using LED-generated white light with a power of ~100 mW/cm^2 under a pure nitrogen atmosphere (O_2 and H_2O levels of <1 ppm). Half of each sample was protected by black and chemically inert plastic, so heat became the main stress factor for the shaded parts of the samples. The stabilized temperature on the surface of the samples in the aging chamber was 40 ± 4 °C. A more detailed description of the experimental setup can be found in our previous reports [46,47].

The degradation behavior of the samples was monitored by taking periodic measurements of their UV–vis absorption spectra using a fiber spectrometer integrated into the glove box. Figure 2 shows the evolution of the absorption profiles of the samples during the heat- or light-induced aging. The reference $MAPbI_3$ films underwent substantial heat-induced degradation, as can be concluded from the decay in the intensity of the perovskite absorption band at 600–800 nm after 1150 h of aging (Figure 2a). On the contrary, the modified $NAd_2MA_{39}Pb_{40}I_{119}Cl_2$ films showed no signs of thermal degradation under the same conditions (Figure 2b). This result indicates that the introduction of **NAdCl** remarkably improved the thermal stability of the $MAPbI_3$ films, which might be explained by the surface covering of the perovskite grains suppressing the loss of volatile perovskite decomposition products and facilitating their recombination and defect healing [46].

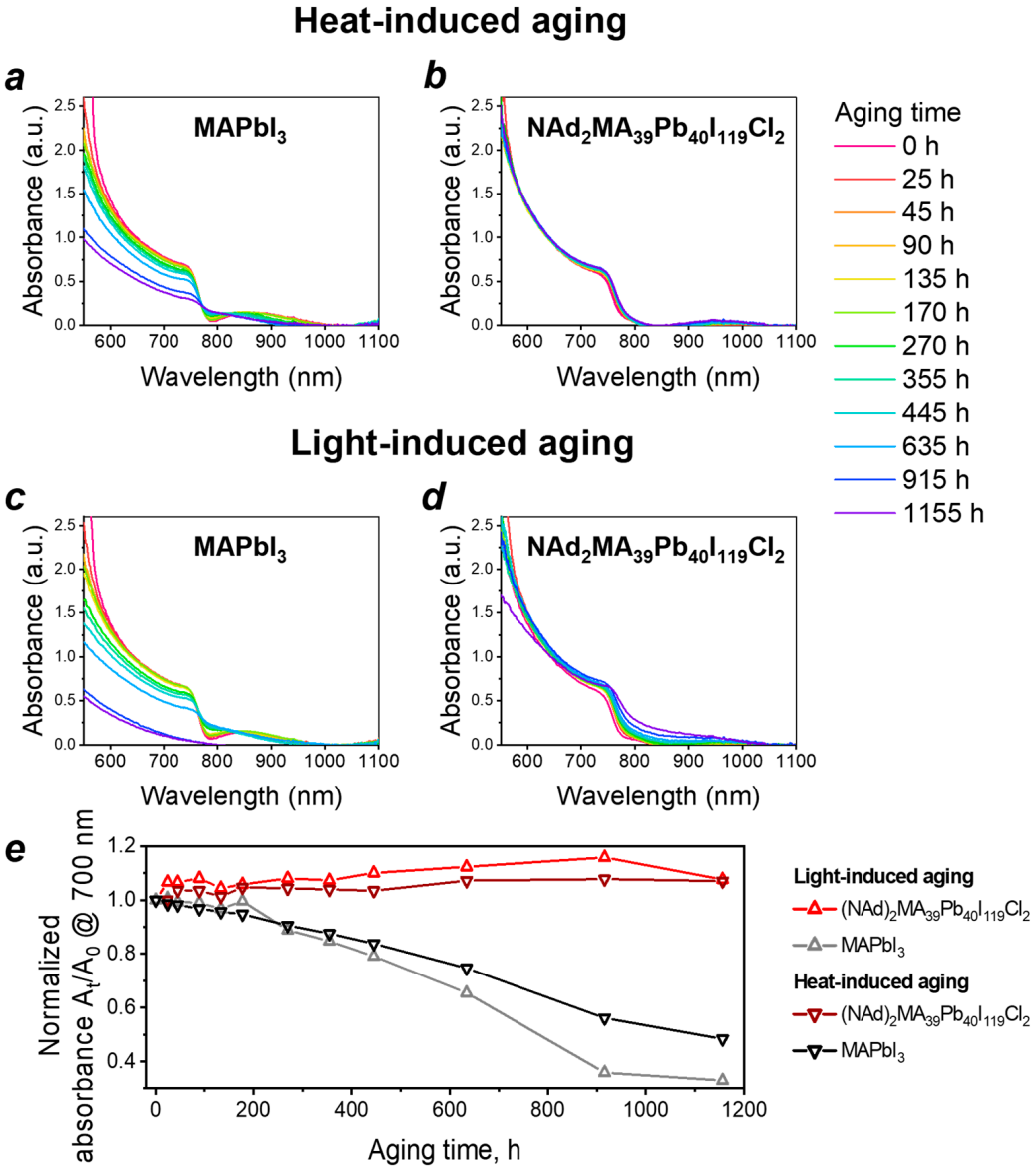

Figure 2. The behavior of the UV–vis spectra of (**a**,**c**) $MAPbI_3$ and (**b**,**d**) $NAd_2MA_{39}Pb_{40}I_{119}Cl_2$ films in the course of (**a**,**b**) heat-induced and (**c**,**d**) light-induced aging. (**e**) The comparison of the degradation dynamics of the samples is based on the evolution of the relative absorbance of the films (A_t/A_0) at 700 nm as a function of the aging time t.

Most importantly, the $NAd_2MA_{39}Pb_{40}I_{119}Cl_2$ films demonstrated remarkably enhanced photostability: the absorption spectrum evolved mostly due to the appearance of a "scattering tail" at 800–1050 nm, which might be associated with the light-induced crystallization of the material [48]. On the contrary, the reference $MAPbI_3$ films underwent almost complete photobleaching at 600–800 nm after 1150 h of light exposure, suggesting that the perovskite phase severely degraded. A comparison of the degradation dynamics of the $MAPbI_3$ and $NAd_2MA_{39}Pb_{40}I_{119}Cl_2$ films is given in Figure 2e by plotting the evolution of the relative absorbance of the films (A_t/A_0) at 700 nm as a function of the aging time. It can be seen from the figure that $NAd_2MA_{39}Pb_{40}I_{119}Cl_2$ films did not significantly change their absorbance at the characteristic perovskite absorption wavelength, in contrast to $MAPbI_3$ films, which underwent severe heat- and light-induced bleaching. Thus, the obtained results reveal **NAdCl** as a highly promising molecular modifier strongly improving both the intrinsic thermal and photochemical stability of the $MAPbI_3$ perovskite films.

The optical spectroscopy data were supplemented by analysis of the X-ray diffraction (XRD) patterns of pristine samples and the films subjected to heat- and light-induced aging

for ~1400 h (Figure 3). The reference $MAPbI_3$ films showed virtually complete heat-induced decomposition with the formation of PbI_2 as a sole product.

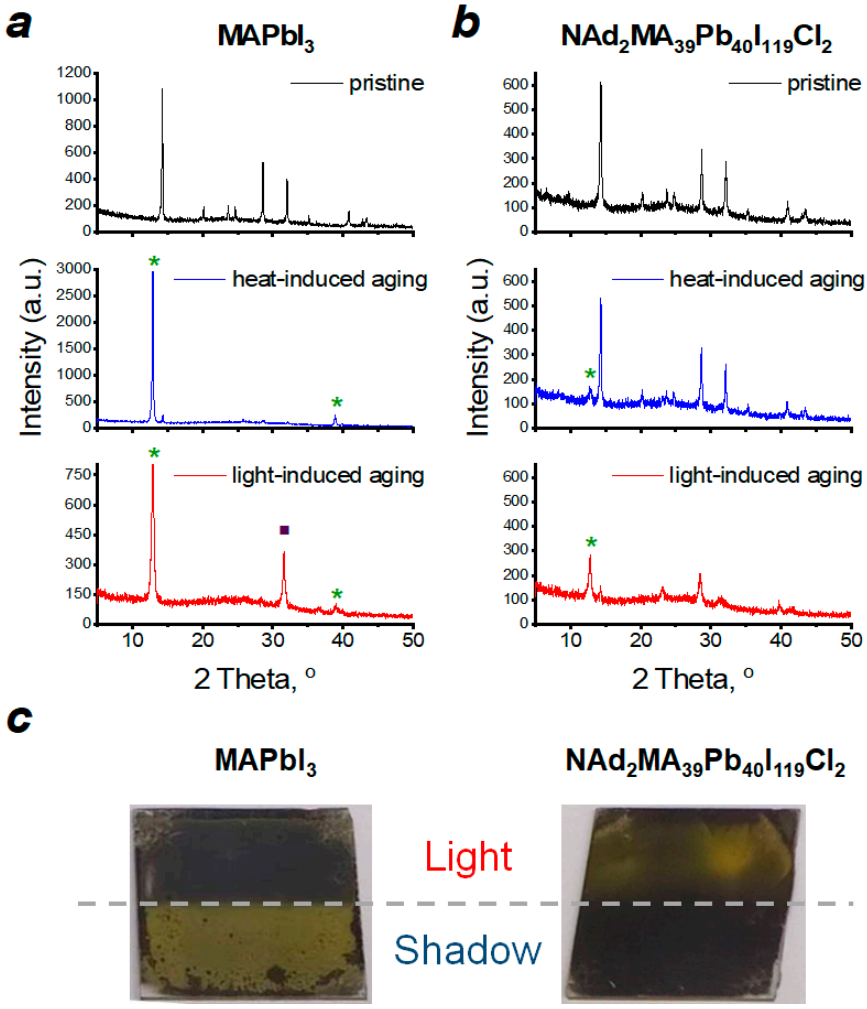

Figure 3. The XRD patterns of the pristine and the thermally and photochemically aged samples of (**a**) $MAPbI_3$ and (**b**) $NAd_2MA_{39}Pb_{40}I_{119}Cl_2$; the peaks of PbI_2 are indicated by "*", and the peaks of Pb^0 are marked with "■". (**c**) The visual appearance of the samples exposed to light or heat (shaded part) after 1400 h of continuous aging.

However, the light-induced aging of $MAPbI_3$ produced PbI_2 and metallic lead Pb^0 appearing with comparable diffraction peak intensities on the XRD pattern (Figure 3a). These results are fully consistent with the previously established thermal and photochemical decomposition pathways of $MAPbI_3$ [10–13,46]. The XRD patterns of $NAd_2MA_{39}Pb_{40}I_{119}Cl_2$ films (Figure 3b) revealed almost no heat-induced degradation (only a minor peak of PbI_2 appeared). The light soaking of $NAd_2MA_{39}Pb_{40}I_{119}Cl_2$ resulted in a pronounced amorphization of the films and a change of their texture, as can be concluded from the suppressed intensity of the diffraction peak at 14.3° and enhanced 28.7° peak. The light-induced aging of $NAd_2MA_{39}Pb_{40}I_{119}Cl_2$ produced PbI_2, as can be concluded from a broad peak at 12.8°, while metallic lead was not formed, which is an important finding.

The XRD data are fully consistent with the visual appearance of the aged samples. The photographs (Figure 3c) show that the reference $MAPbI_3$ films became yellow in the shaded part (PbI_2 formation) and grey in the part exposed to light (due to metallic lead Pb^0 formation). On the contrary, the $NAd_2MA_{39}Pb_{40}I_{119}Cl_2$ films stayed black in the shadow (the perovskite survived thermal aging) and became inhomogeneously yellowish upon light exposure (perovskite was partially converted to PbI_2). The obtained results indicate

that the introduction of **NAdCl** not only improved the perovskite film stability but also altered the film's light-induced degradation pathways, which is a crucially important finding potentially helping to improve the operational lifetime of perovskite photovoltaics.

The degradation behavior of the studied perovskite formulations was additionally assessed using X-ray photoelectron spectroscopy (XPS). The XPS Pb $4f_{7/2}$ spectra of the reference $MAPbI_3$ films showed strong high-energy shifts after the heat-induced and, in particular, the light-induced aging, which is consistent with the accumulation of PbI_2 as the main aging product (Figure 4a).

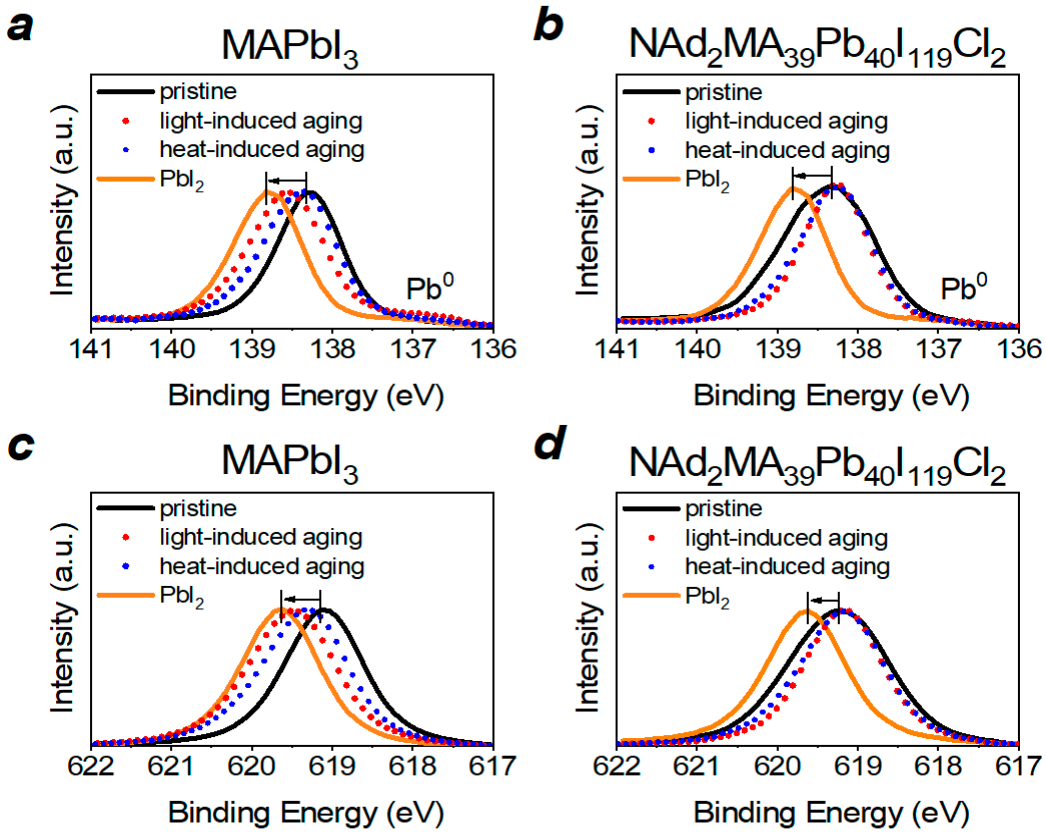

Figure 4. The (**a**,**b**) Pb $4f_{7/2}$ and (**c**,**d**) I $3d_{5/2}$ spectra of pristine and thermally and photochemically aged samples of (**a**,**c**) $MAPbI_3$ and (**b**,**d**) $NAd_2MA_{39}Pb_{40}I_{119}Cl_2$.

The formation of PbI_2 is also consistent with the behavior of the XPS I $3d_{5/2}$ band, which underwent a high-energy shift upon thermal or photochemical aging of the samples (Figure 4c). Interestingly, we observed only a small contribution of Pb^0 to the XPS Pb $4f_{7/2}$ spectra of the $MAPbI_3$ films exposed to light, whereas XRD revealed the formation of substantial amounts of metallic lead. This apparent contradiction can be explained by the formation of metallic lead mostly in the bulk of the films rather than on the film surface, which was selectively probed by XPS. The XPS spectra of the $NAd_2MA_{39}Pb_{40}I_{119}Cl_2$ films showed no high-energy shifts due to PbI_2 formation (Figure 4b,d), which matches the UV–vis and XRD data revealing the superior stability of this perovskite formulation.

The UV–vis spectroscopy, XRD, and XPS data presented above unambiguously prove that introduction of the **NAdCl** modifier strongly enhanced the intrinsic thermal and photochemical stability of the $MAPbI_3$ perovskite films. The observed stabilization effect might be related to the passivation of defects localized mostly at the grain boundaries. It is known from the literature that such defects can behave as traps for, e.g., positive charge carriers, which degrade the material with the formation of molecular iodine (I_2) or triiodide (I_3^-) [49]. The concentration of defects strongly affects the recombination of charge carriers. However, the predominant charge carrier recombination pathway can be

deduced by considering the dependence of the photoluminescence (PL) intensity on the power of the excitation beam [50]. We performed such experiments (Figure 5) and showed that both the $MAPbI_3$ and $NAd_2MA_{39}Pb_{40}I_{119}Cl_2$ films had good electronic quality.

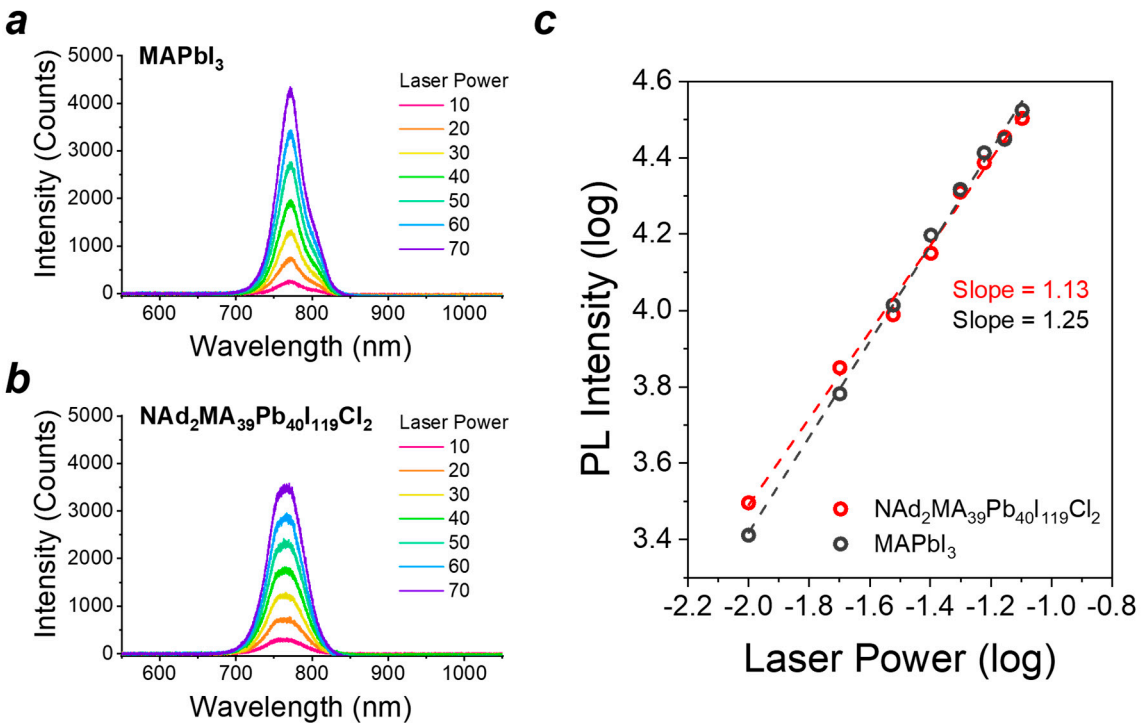

Figure 5. The evolution of the PL spectra of (**a**) $MAPbI_3$ and (**b**) $NAd_2MA_{39}Pb_{40}I_{119}Cl_2$ with increasing laser power (given in μW). (**c**) The PL intensity versus the laser power double logarithmic dependence was used to obtain the characteristic slope (S) values.

Still, the introduction of **NAdCl** modifier decreased the slope (S) of the $\log(I_{PL})$ vs. $\log(P_{ex})$ dependence from 1.25 to 1.13, which is consistent with a significant reduction in the concentration of traps. It should be emphasized that the bimolecular charge recombination pathway strongly dominates over trap-assisted recombination for the perovskite films with S = 1.13. Suppressed trap-assisted recombination in the perovskite films directly translates to enhanced photostability, as we have shown recently [51].

A particularly important finding is the fact that **NAdCl** modifier prevented the formation of metallic lead as a product of light-induced degradation of perovskite films. The mechanism behind this effect is not clear at the moment. We hypothesize that $\mathbf{NAd}^+$ cations interact efficiently with the surrounding ions in the perovskite framework, involving efficient coordination and hydrogen bonding. This hypothesis is supported by the fact that the XPS N 1s band of the pristine $NAd_2MA_{39}Pb_{40}I_{119}Cl_2$ sample became considerably broader and underwent a low-energy shift by ~0.3 eV as compared to the spectrum of the freshly deposited reference $MAPbI_3$ film (Figure 6a).

Similar electronic effects were observed in XPS spectra and were reported previously [52,53] as signatures of strong electronic interactions between the introduced molecular modifier and the entire perovskite framework. We believe that these interactions induce a strong stabilization effect on Pb^{2+} cations (particularly the ones with an unsaturated coordination environment), which suppresses their reduction to Pb^0 via electron trapping. Indeed, the XPS Pb $4f_{7/2}$ band also shifted by ~0.1 eV to higher energy, which supports the existence of some electronic interactions of Pb^{2+} with $\mathbf{NAd}^+$ (Figure 6b). Similar observations were reported recently for $MAPbI_3$ films passivated using pentaerythritol tetrakis(3-mercaptopropionate) as a molecular modifier [52].

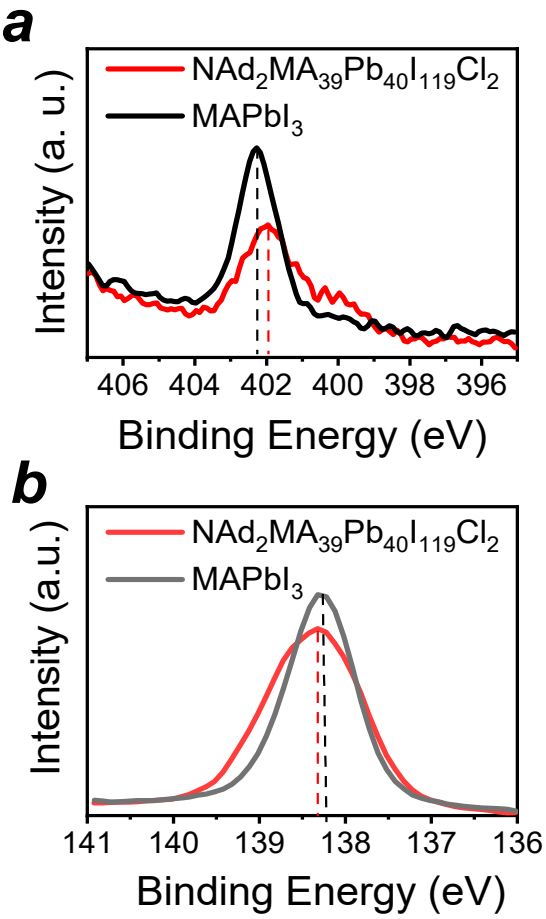

Figure 6. XPS (**a**) N 1s and (**b**) Pb $4f_{7/2}$ spectra of pristine films of $MAPbI_3$ and $NAd_2MA_{39}Pb_{40}I_{119}Cl_2$.

3. Discussion

We introduced herein the 1,4,6,10-tetraazaadamantane derivative **NAdCl** as a promising molecular modifier for $MAPbI_3$ films. The incorporation of **NAdCl** dramatically improved the thermal and photochemical stability of the perovskite films, as revealed using a set of complementary analytical techniques. The observed effects are consistent with the hypothesis that bulky $\mathbf{NAd}^+$ cations are mostly localized at the surface of the perovskite grains and grain boundaries, thus providing an efficient surface covering suppressing the loss of volatile perovskite decomposition products. Furthermore, the introduction of **NAdCl** improved the electronic quality of the perovskite films and suppressed trap-assisted recombination of charge carriers, which is a major pathway leading to material degradation (trapping holes or electrons launches a series of parasitic redox reactions). Most importantly, **NAdCl** prevented the formation of metallic lead as the perovskite photodegradation product, which might allow the lifetime of perovskite absorber materials and the corresponding solar cells to be extended. This effect most likely originates from strong interactions of $\mathbf{NAd}^+$ cations with undercoordinated Pb^{2+} ions at the grain surface, which results in healing of the traps for electrons and suppression of the parasitic redox reaction $Pb^{2+} + 2e \Rightarrow Pb^0$.

Importantly, the perovskite solar cells assembled in the n–i–p configuration ITO/SnO_2/PCBA/perovskite/PTAA/MoO_3/Ag (ITO is indium-tin oxide; PCBA is phenyl-C_{61}-butyric acid; PTAA is poly[bis(4-phenyl)(2,5,6-trimethylphenyl)amine) following a procedure reported previously [54] and with the optimal loading of **NAdCl**, showed decent photovoltaic characteristics: open-circuit voltage (V_{OC}) of 1045 mV, short-circuit current density (J_{SC}) of 23.1 mA/cm^2, fill factor (FF) of 63.4%, and power conversion efficiency (PCE) of 15.5% as extracted from the reverse scan of the current–voltage characteristics. The forward scan pro-

vided very similar parameters: V_{OC} = 1047 mV, J_{SC} = 23.3 mA/cm^2, FF = 60.8%, and PCE = 14.8%. These results also indicate small hysteresis in the current–voltage characteristics, as shown in Figure 7.

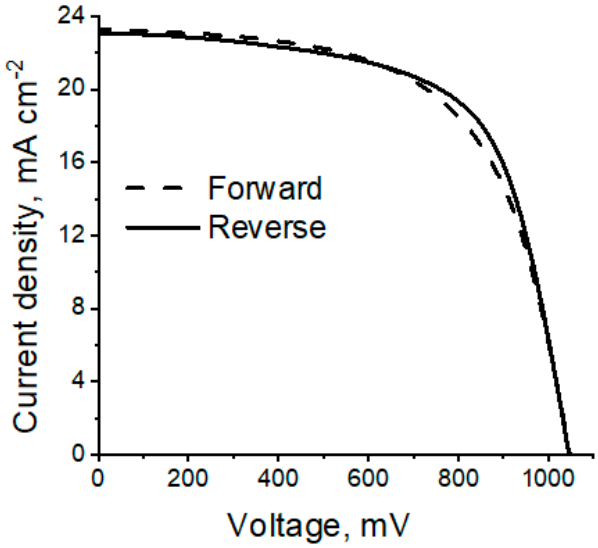

Figure 7. The current–voltage characteristics of the ITO/SnO_2/PCBA/perovskite/PTAA/MoO_3/Ag perovskite solar cell, where the perovskite is represented by $MAPbI_3$ loaded with 0.025% of **NAdCl.**

The overall set of obtained results features 1,4,6,10-tetraazaadamantane derivatives as a highly promising family of molecular modifiers for perovskite-type absorber materials, deserving of further systematic exploration.

4. Materials and Methods

4.1. Materials

Lead iodide (PbI_2, 99.99%) and methylammonium iodide (MAI, 99.9%) were purchased from FOMaterials Ltd. (Chernogolovka, Russia). Anhydrous dimethylformamide (DMF) and chlorobenzene were purchased from Sigma-Aldrich and used as received inside nitrogen glove boxes. Glass slides (25 × 25 mm) were cut from standard objective borosilicate glass purchased from Isolab GmbH.

4.2. Synthesis and Characterization of 4,6,10-Trihydroxy-3,5,7-Trimethyl-1,4,6,10-Tetraazaadamantan-1-Ium Chloride (NAdCl)

The title compound was synthesized using a two-step literature method [38], which was modified for gram-scale preparation.

Step 1. Concentrated ammonia solution (ca. 25% in water, 25 mL, 316 mmol) was added to a solution of hydroxylamine hydrochloride (4.38 g, 63 mmol) in water (25 mL) at 0 °C. To the resulting solution, chloroacetone (5.0 mL, 62 mmol) was slowly added upon intensive stirring (the reaction is exothermic). The cooling bath was removed and the reaction mixture was stirred for 1 h at room temperature. The white precipitate of 1,1′,1″-nitrilotris(propan-2-one) trioxime (**TRISOXH3**) was collected by filtration, washed with water and diethyl ether, and dried in vacuum. Yield: 1.4 g (30%).

Step 2. Glacial acetic acid (0.9 mL, 15.8 mmol) was added to a suspension of **TRISOXH3** (1.15 g, 5 mmol) in methanol (20 mL) at room temperature. The mixture was stirred overnight until the complete conversion of **TRISOXH3** was observed (controlled by thin-layer chromatography). The resulting solution was carefully treated with concentrated hydrochloric acid (ca. 36% in water, 0.45 mL, 5.2 mmol) at room temperature (precipitation of **NAdCl** takes place) and kept in a fridge (0–5 °C) for several hours. The precipitate of **NAdCl** was collected, rinsed with a small amount of methanol, and dried in vacuum until constant weight. Yield: 1.05 g (79% from **TRISOXH3**). White crystalline solid. Mp 181–

184 °C (with decomp.) (lit. [38] 181–183 °C). ^{1}H NMR (300 MHz, D_2O, 24 °C): δ 1.25 (singlet, 9H, 3 CH_3), 3.41–3.53 (broad singlet, 6H, 3 CH_2), 3 NOH and NH were not observed due to the proton–deuterium exchange process. The NMR spectrum was in agreement with literature data [38].

4.3. Preparation of the $MAPbI_3$ and $NAd_2MA_{39}Pb_{40}I_{119}Cl_2$ Films

$MAPbI_3$ precursor solution with a final concentration of 1.35 M was obtained by dissolving together equimolar amounts of MAI and PbI_2 in anhydrous DMF by continuous stirring at 70 °C. The $NAd_2MA_{39}Pb_{40}I_{119}Cl_2$ precursor solution was obtained by dissolving 18.4 mg of **NAdCl**, 214.6 mg of MAI, and 638.4 mg of PbI_2 in 1 mL of DMF by continuous stirring at 70 °C. Both prepared solutions were filtered through 0.45 μm PTFE syringe filters before spin coating, though they were transparent and showed no signs of undissolved solids before the filtration. A 55 μL aliquot of the corresponding precursor solution was dropped on a glass substrate rotating at 3000 rpm and then quenched after 8–9 s by dripping 120 μL of anhydrous chlorobenzene. The sample was kept at 3000 rpm for an additional 40 s and then annealed at 100 °C on a hot plate for 5 min. All aforementioned operations were performed in an inert atmosphere inside nitrogen-filled MBraun glove boxes. A few samples from every batch of the prepared films were characterized by XRD to confirm their phase purity before starting the aging experiments.

4.4. Aging Experiments

Aging experiments were performed in a pure nitrogen atmosphere inside an MBraun glove box (O_2 and H_2O levels below 1 ppm) using a specially designed white light chamber [39]. An LED array provided light flux of 100 ± 5 mW/cm^2. Half of each sample was exposed to light, whereas the other half was shaded by a chemically inert plastic holder. Such an experimental design allowed us to investigate both heat-induced and light-induced aging pathways on the same glass slide. The samples loaded in the aging chamber were cooled by multiple fans fixed at the back of the sample holder, which provided an equilibrium temperature of 40 ± 4 °C as measured by a thermocouple and non-contact IR thermometer on the sample surface. The samples were periodically characterized by taking UV–vis spectroscopy measurements in the same glove box without exposure to the ambient atmosphere.

4.5. Characterization Techniques

Steady-state PL spectra were measured under a nitrogen atmosphere using a Horiba spectrometer and a 532 nm laser as the excitation source. UV–vis spectra, XRD patterns, and XPS spectra were obtained using an AvaSpec-2048-2UV-VIS fiber spectrometer, Bruker D8 instrument with a Cu Kα source, and PHI 5000 Versa Probe spectrometer (ULVAC-Physical Electronics, Chanhassen, USA), respectively, following previously reported procedures [40]. The samples for XRD characterization were coated with polystyrene films inside the glove box to protect them from aging under ambient conditions during the measurement (5–7 min). The samples for XPS measurements were sealed in airtight Al-coated plastic foil envelopes during transportation. Opening the envelopes and loading the samples in the spectrometer chamber was done within 1–3 min to minimize the samples' exposure to air.

Author Contributions: P.A.T. and S.M.A. conceptualized and designed the performed experiments. V.V.O. performed a major part of the work related to sample preparation and aging experiments. I.S.Z. and E.Z.K. performed XPS studies. A.B. performed and interpreted PL measurements. N.N.D. performed SEM measurements. G.V.S. organized XRD studies and participated in analysis of the data. N.A.E. performed AFM studies. A.Y.S. provided the **NAdCl** modifier for this study. L.A.F. and P.A.T. participated in the supervision of the work. All authors contributed to the discussion and writing the original draft of the paper. All authors have read and agreed to the published version of the manuscript.

Funding: This work was supported by Russian Science Foundation (project No. 19-73-30020). The XPS measurements were supported by the Ministry of Education and Science of the Russian Federation (project FEUZ-2020-0060), Theme 'Electron', no. AAAA-A18-118020190098-5 and Russian Foundation for Basic Research (project No. 21-52-52002).

Acknowledgments: We thank S. Shapaeva for support with the XRD measurements at IPCP RAS.

Conflicts of Interest: The authors declare no conflict of interest.

References

1. NREL Efficiency Chart. Available online: https://www.nrel.gov/pv/cell-efficiency.html (accessed on 27 January 2021).
2. Al-Ashouri, A.; Köhnen, E.; Li, B.; Magomedov, A.; Hempel, H.; Caprioglio, P.; Márquez, J.A.; Morales Vilches, A.B.; Kasparavicius, E.; Smith, J.A.; et al. Monolithic Perovskite/Silicon Tandem Solar Cell with >29% Efficiency by Enhanced Hole Extraction. *Science* **2020**, *370*, 1300–1309. [CrossRef] [PubMed]
3. Meng, L.; You, J.; Yang, Y. Addressing the Stability Issue of Perovskite Solar Cells for Commercial Applications. *Nat. Commun.* **2018**, *9*, 5265. [CrossRef] [PubMed]
4. Leguy AM, A.; Hu, Y.; Campoy-Quiles, M.; Alonso, M.I.; Weber, O.J.; Azarhoosh, P.; van Schilfgaarde, M.; Weller, M.T.; Bein, T.; Nelson, J.; et al. Reversible Hydration of $CH_3NH_3PbI_3$ in Films, Single Crystals, and Solar Cells. *Chem. Mater.* **2015**, *27*, 3397–3407. [CrossRef]
5. Bryant, D.; Aristidou, N.; Pont, S.; Sanchez-Molina, I.; Chotchunangatchaval, T.; Wheeler, S.; Durrant, J.R.; Haque, S.A. Light and Oxygen Induced Degradation Limits the Operational Stability of Methylammonium Lead Triiodide Perovskite Solar Cells. *Energy Environ. Sci.* **2016**, *9*, 1655–1660. [CrossRef]
6. Nayakasinghe, M.T.; Han, Y.; Sivapragasam, N.; Kilin, D.S.; Burghaus, U. Unexpected High Binding Energy of CO_2 on $CH_3NH_3PbI_3$ Lead-Halide Organic–Inorganic Perovskites *via* Bicarbonate Formation. *Chem. Commun.* **2018**, *54*, 9949–9952. [CrossRef] [PubMed]
7. Singh, R.; Sandhu, S.; Yadav, H.; Lee, J.-J. Stable Triple-Cation (Cs^+ –MA^+ –FA^+) Perovskite Powder Formation under Ambient Conditions for Hysteresis-Free High-Efficiency Solar Cells. *ACS Appl. Mater. Interfaces* **2019**, *11*, 29941–29949. [CrossRef]
8. Shekargoftar, M.; Jurmanová, J.; Homola, T. A Study on the Effect of Ambient Air Plasma Treatment on the Properties of Methylammonium Lead Halide Perovskite Films. *Metals* **2019**, *9*, 991. [CrossRef]
9. Brunetti, B.; Cavallo, C.; Ciccioli, A.; Gigli, G.; Latini, A. On the Thermal and Thermodynamic (In)Stability of Methylammonium Lead Halide Perovskites. *Sci. Rep.* **2016**, *6*, 31896. [CrossRef]
10. Juarez-Perez, E.J.; Hawash, Z.; Raga, S.R.; Ono, L.K.; Qi, Y. Thermal Degradation of $CH_3NH_3PbI_3$ Perovskite into NH_3 and CH_3I Gases Observed by Coupled Thermogravimetry–Mass Spectrometry Analysis. *Energy Environ. Sci.* **2016**, *9*, 3406–3410. [CrossRef]
11. Akbulatov, A.F.; Martynenko, V.M.; Frolova, L.A.; Dremova, N.N.; Zhidkov, I.; Tsarev, S.A.; Luchkin, S.Y.; Kurmaev, E.Z.; Aldoshin, S.M.; Stevenson, K.J.; et al. Intrinsic Thermal Decomposition Pathways of Lead Halide Perovskites $APbX_3$. *Solar Energy Mater. Solar Cells* **2020**, *213*, 110559. [CrossRef]
12. Juarez-Perez, E.J.; Ono, L.K.; Maeda, M.; Jiang, Y.; Hawash, Z.; Qi, Y. Photodecomposition and Thermal Decomposition in Methylammonium Halide Lead Perovskites and Inferred Design Principles to Increase Photovoltaic Device Stability. *J. Mater. Chem. A* **2018**, *6*, 9604–9612. [CrossRef]
13. Akbulatov, A.F.; Luchkin, S.Y.u.; Frolova, L.A.; Dremova, N.N.; Gerasimov, K.L.; Zhidkov, I.S.; Anokhin, D.V.; Kurmaev, E.Z.; Stevenson, K.J.; Troshin, P.A. Probing the Intrinsic Thermal and Photochemical Stability of Hybrid and Inorganic Lead Halide Perovskites. *J. Phys. Chem. Lett.* **2017**, *8*, 1211–1218. [CrossRef] [PubMed]
14. Misra, R.K.; Aharon, S.; Li, B.; Mogilyansky, D.; Visoly-Fisher, I.; Etgar, L.; Katz, E.A. Temperature-and Component-Dependent Degradation of Perovskite Photovoltaic Materials under Concentrated Sunlight. *J. Phys. Chem. Lett.* **2015**, *6*, 326–330. [CrossRef] [PubMed]
15. Zhang, Z.; Wu, J.; Li, S.; Liu, S.; Wang, Q.; Mei, A.; Rong, Y.; Han, H.; Hu, Y. Progress in Multifunctional Molecules for Perovskite Solar Cells. *Sol. RRL* **2020**, *4*, 1900248. [CrossRef]
16. Mahapatra, A.; Prochowicz, D.; Tavakoli, M.M.; Trivedi, S.; Kumar, P.; Yadav, P. A Review of Aspects of Additive Engineering in Perovskite Solar Cells. *J. Mater. Chem. A* **2020**, *8*, 27–54. [CrossRef]
17. Gao, F.; Zhao, Y.; Zhang, X.; You, J. Recent Progresses on Defect Passivation toward Efficient Perovskite Solar Cells. *Adv. Energy Mater.* **2020**, *10*, 1902650. [CrossRef]
18. Aydin, E.; Bastiani, M.; Wolf, S. Defect and Contact Passivation for Perovskite Solar Cells. *Adv. Mater.* **2019**, *31*, 1900428. [CrossRef]
19. Singh, R.; Ryu, I.; Yadav, H.; Park, J.; Jo, J.W.; Yim, S.; Lee, J.-J. Non-Hydrolytic Sol-Gel Route to Synthesize TiO_2 Nanoparticles under Ambient Condition for Highly Efficient and Stable Perovskite Solar Cells. *Solar Energy* **2019**, *185*, 307–314. [CrossRef]
20. Chen, L.-C.; Tien, C.-H.; Jhou, Y.-C.; Lin, W.-C. Co-Solvent Controllable Engineering of $MA_{0.5}FA_{0.5}Pb_{0.8}Sn_{0.2}I_3$ Lead–Tin Mixed Perovskites for Inverted Perovskite Solar Cells with Improved Stability. *Energies* **2020**, *13*, 2438. [CrossRef]
21. Milić, J.V.; Kubicki, D.J.; Emsley, L.; Grätzel, M. Multifunctional Molecular Modulation for Efficient and Stable Hybrid Perovskite Solar Cells. *Chimia* **2019**, *73*, 317–323. [CrossRef]
22. Yang, S.; Wang, Y.; Liu, P.; Cheng, Y.-B.; Zhao, H.J.; Yang, H.G. Functionalization of Perovskite Thin Films with Moisture-Tolerant Molecules. *Nat. Energy* **2016**, *1*, 15016. [CrossRef]

23. Kim, H.; Lee, S.; Lee, D.Y.; Paik, M.J.; Na, H.; Lee, J.; Seok, S.I. Optimal Interfacial Engineering with Different Length of Alkylammonium Halide for Efficient and Stable Perovskite Solar Cells. *Adv. Energy Mater.* **2019**, *9*, 1902740. [CrossRef]
24. Jung, M.; Shin, T.J.; Seo, J.; Kim, G.; Seok, S.I. Structural Features and Their Functions in Surfactant-Armoured Methylammonium Lead Iodide Perovskites for Highly Efficient and Stable Solar Cells. *Energy Environ. Sci.* **2018**, *11*, 2188–2197. [CrossRef]
25. Guo, P.; Ye, Q.; Yang, X.; Zhang, J.; Xu, F.; Shchukin, D.; Wei, B.; Wang, H. Surface & Grain Boundary Co-Passivation by Fluorocarbon Based Bifunctional Molecules for Perovskite Solar Cells with Efficiency over 21%. *J. Mater. Chem. A* **2019**, *7*, 2497–2506. [CrossRef]
26. Ali, N.; Wang, X.; Rauf, S.; Attique, S.; Khesro, A.; Ali, S.; Mushtaq, N.; Xiao, H.; Yang, C.P.; Wu, H. Enhanced Stability in Cesium Assisted Hybrid 2D/3D-Perovskite Thin Films and Solar Cells Prepared in Ambient Humidity. *Solar Energy* **2019**, *189*, 325–332. [CrossRef]
27. Liu, Y.; Akin, S.; Pan, L.; Uchida, R.; Arora, N.; Milić, J.V.; Hinderhofer, A.; Schreiber, F.; Uhl, A.R.; Zakeeruddin, S.M.; et al. Ultrahydrophobic 3D/2D Fluoroarene Bilayer-Based Water-Resistant Perovskite Solar Cells with Efficiencies Exceeding 22%. *Sci. Adv.* **2019**, *5*, eaaw2543. [CrossRef] [PubMed]
28. Abbas, M.S.; Hussain, S.; Zhang, J.; Wang, B.; Yang, C.; Wang, Z.; Wei, Z.; Ahmad, R. Orientationally Engineered 2D/3D Perovskite for High Efficiency Solar Cells. *Sustain. Energy Fuels* **2020**, *4*, 324–330. [CrossRef]
29. Rodríguez-Romero, J.; Hames, B.C.; Mora-Seró, I.; Barea, E.M. Conjugated Organic Cations to Improve the Optoelectronic Properties of 2D/3D Perovskites. *ACS Energy Lett.* **2017**, *2*, 1969–1970. [CrossRef]
30. Zheng, H.; Liu, G.; Zhu, L.; Ye, J.; Zhang, X.; Alsaedi, A.; Hayat, T.; Pan, X.; Dai, S. The Effect of Hydrophobicity of Ammonium Salts on Stability of Quasi-2D Perovskite Materials in Moist Condition. *Adv. Energy Mater.* **2018**, *8*, 1800051. [CrossRef]
31. Li, S.; Hu, L.; Zhang, C.; Wu, Y.; Liu, Y.; Sun, Q.; Cui, Y.; Hao, Y.; Wu, Y. In Situ Growth of a 2D/3D Mixed Perovskite Interface Layer by Seed-Mediated and Solvent-Assisted Ostwald Ripening for Stable and Efficient Photovoltaics. *J. Mater. Chem. C* **2020**, *8*, 2425–2435. [CrossRef]
32. Tavakoli, M.M.; Bi, D.; Pan, L.; Hagfeldt, A.; Zakeeruddin, S.M.; Grätzel, M. Adamantanes Enhance the Photovoltaic Performance and Operational Stability of Perovskite Solar Cells by Effective Mitigation of Interfacial Defect States. *Adv. Energy Mater.* **2018**, *8*, 1800275. [CrossRef]
33. Tavakoli, M.M.; Tress, W.; Milić, J.V.; Kubicki, D.; Emsley, L.; Grätzel, M. Addition of Adamantylammonium Iodide to Hole Transport Layers Enables Highly Efficient and Electroluminescent Perovskite Solar Cells. *Energy Environ. Sci.* **2018**, *11*, 3310–3320. [CrossRef]
34. Tavakoli, M.M.; Yadav, P.; Prochowicz, D.; Sponseller, M.; Osherov, A.; Bulović, V.; Kong, J. Controllable Perovskite Crystallization via Antisolvent Technique Using Chloride Additives for Highly Efficient Planar Perovskite Solar Cells. *Adv. Energy Mater.* **2019**, *9*, 1803587. [CrossRef]
35. Milić, J.V.; Im, J.; Kubicki, D.J.; Ummadisingu, A.; Seo, J.; Li, Y.; Ruiz-Preciado, M.A.; Dar, M.I.; Zakeeruddin, S.M.; Emsley, L.; et al. Supramolecular Engineering for Formamidinium-Based Layered 2D Perovskite Solar Cells: Structural Complexity and Dynamics Revealed by Solid-State NMR Spectroscopy. *Adv. Energy Mater.* **2019**, *9*, 1900284. [CrossRef]
36. Martínez-Sarti, L.; Palazon, F.; Sessolo, M.; Bolink, H.J. Dry Mechanochemical Synthesis of Highly Luminescent, Blue and Green Hybrid Perovskite Solids. *Adv. Optical Mater.* **2020**, *8*, 1901494. [CrossRef]
37. Zheng, Y.-Z.; Li, X.-T.; Zhao, E.-F.; Lv, X.-D.; Meng, F.-L.; Peng, C.; Lai, X.-S.; Huang, M.; Cao, G.; Tao, X.; et al. Hexamethylenetetramine-Mediated Growth of Grain-Boundary-Passivation $CH_3NH_3PbI_3$ for Highly Reproducible and Stable Perovskite Solar Cells. *J. Power Sources* **2018**, *377*, 103–109. [CrossRef]
38. Semakin, A.N.; Sukhorukov, A.Y.; Lesiv, A.V.; Ioffe, S.L.; Lyssenko, K.A.; Nelyubina, Y.V.; Tartakovsky, V.A. Unusual Intramolecular Cyclization of Tris(β-oximinoalkyl)amines. The First Synthesis of 1,4,6,10-Tetraazaadamantanes. *Org. Lett.* **2009**, *11*, 4072–4075. [CrossRef]
39. Tolbin, A.Y.; Sukhorukov, A.Y.; Ioffe, S.L.; Lobach, O.A.; Nosik, D.N.; Tomilova, L.G. Synthesis of a Phtalocyanine -1,4,6,10-Tetraazaadamantane Conjugate and Its Activity Against the Human Immunodeficiency Virus. *Mendeleev Commun.* **2010**, *20*, 24–26. [CrossRef]
40. Golovanov, I.S.; Mazeina, G.S.; Nelyubina, Y.V.; Novikov, R.A.; Mazur, A.S.; Britvin, S.N.; Tartakovsky, V.A.; Ioffe, S.L.; Sukhorukov, A.Y. Exploiting Coupling of Boronic Acids with Triols for a pH-Dependent "Click-Declick" Chemistry. *J. Org. Chem.* **2018**, *83*, 9756–9773. [CrossRef]
41. Premužič, D.; Hołynska, M.; Ozarowski, A.; Pietzonka, C.; Roseborough, A.; Stoian, S.A. Model Dimeric Manganese(IV) Complexes Featuring Terminal Trishydroxotetraazaadamantane and Various Bridging Ligands. *Inorg. Chem.* **2020**, *59*, 10768–10784. [CrossRef]
42. Cohen, B.-E.; Wierzbowska, M.; Etgar, L. High Efficiency and High Open Circuit Voltage in Quasi 2D Perovskite Based Solar Cells. *Adv. Funct. Mater.* **2017**, *27*, 1604733. [CrossRef]
43. Quan, L.N.; Yuan, M.; Comin, R.; Voznyy, O.; Beauregard, E.M.; Hoogland, S.; Buin, A.; Kirmani, A.R.; Zhao, K.; Amassian, A.; et al. Ligand-Stabilized Reduced-Dimensionality Perovskites. *J. Am. Chem. Soc.* **2016**, *138*, 2649–2655. [CrossRef] [PubMed]
44. Chaudhary, B.; Koh, T.M.; Febriansyah, B.; Bruno, A.; Mathews, N.; Mhaisalkar, S.G.; Soci, C. Mixed-Dimensional Naphthylmethylammonium-Methylammonium Lead Iodide Perovskites with Improved Thermal Stability. *Sci. Rep.* **2020**, *10*, 429. [CrossRef] [PubMed]

45. Lee, D.S.; Yun, J.S.; Kim, J.; Soufiani, A.M.; Chen, S.; Cho, Y.; Deng, X.; Seidel, J.; Lim, S.; Huang, S.; et al. Passivation of Grain Boundaries by Phenethylammonium in Formamidinium-Methylammonium Lead Halide Perovskite Solar Cells. *ACS Energy Lett.* **2018**, *3*, 647–654. [CrossRef]
46. Akbulatov, A.F.; Frolova, L.A.; Dremova, N.N.; Zhidkov, I.; Martynenko, V.M.; Tsarev, S.A.; Luchkin, S.Y.; Kurmaev, E.Z.; Aldoshin, S.M.; Stevenson, K.J.; et al. Light or Heat: What Is Killing Lead Halide Perovskites under Solar Cell Operation Conditions? *J. Phys. Chem. Lett.* **2020**, *11*, 333–339. [CrossRef] [PubMed]
47. Boldyreva, A.G.; Akbulatov, A.F.; Elnaggar, M.; Luchkin, S.Y.; Danilov, A.V.; Zhidkov, I.S.; Yamilova, O.R.; Fedotov, Y.S.; Bredikhin, S.I.; Kurmaev, E.Z.; et al. Impact of Charge Transport Layers on the Photochemical Stability of $MAPbI_3$ in Thin Films and Perovskite Solar Cells. *Sustain. Energy Fuels* **2019**, *3*, 2705–2716. [CrossRef]
48. Boldyreva, A.G.; Zhidkov, I.S.; Tsarev, S.; Akbulatov, A.F.; Tepliakova, M.M.; Fedotov, Y.S.; Bredikhin, S.I.; Postnova, E.Y.; Luchkin, S.Y.; Kurmaev, E.Z.; et al. Unraveling the Impact of Hole Transport Materials on Photostability of Perovskite Films and p–i–n Solar Cells. *ACS Appl. Mater. Interfaces* **2020**, *12*, 19161–19173. [CrossRef]
49. Meggiolaro, D.; Motti, S.G.; Mosconi, E.; Barker, A.J.; Ball, J.; Andrea Riccardo Perini, C.; Deschler, F.; Petrozza, A.; De Angelis, F. Iodine Chemistry Determines the Defect Tolerance of Lead-Halide Perovskites. *Energy Environ. Sci.* **2018**, *11*, 702–713. [CrossRef]
50. Draguta, S.; Thakur, S.; Morozov, Y.V.; Wang, Y.; Manser, J.S.; Kamat, P.V.; Kuno, M. Spatially Non-Uniform Trap State Densities in Solution-Processed Hybrid Perovskite Thin Films. *J. Phys. Chem. Lett.* **2016**, *7*, 715–721. [CrossRef]
51. Akbulatov, A.F.; Frolova, L.A.; Tsarev, S.A.; Zhidkov, I.; Luchkin, S.Y.; Kurmaev, E.Z.; Stevenson, K.J.; Aldoshin, S.M.; Troshin, P.A. Film Deposition Techniques Impact the Defect Density and Photostability of $MAPbI_3$ Perovskite Films. *J. Phys. Chem. C* **2020**, *124*, 21378–21385. [CrossRef]
52. Wu, Z.; Jiang, M.; Liu, Z.; Jamshaid, A.; Ono, L.K.; Qi, Y. Highly Efficient Perovskite Solar Cells Enabled by Multiple Ligand Passivation. *Adv. Energy Mater.* **2020**, *10*, 1903696. [CrossRef]
53. Chen, J.; Kim, S.-G.; Ren, X.; Jung, H.S.; Park, N.-G. Effect of Bidentate and Tridentate Additives on the Photovoltaic Performance and Stability of Perovskite Solar Cells. *J. Mater. Chem. A* **2019**, *7*, 4977–4987. [CrossRef]
54. Tsarev, S.; Dubinina, T.S.; Luchkin, S.Y.; Zhidkov, I.S.; Kurmaev, E.Z.; Stevenson, K.J.; Troshin, P.A. Phenyl-C_{61} -Butyric Acid as an Interface Passivation Layer for Highly Efficient and Stable Perovskite Solar Cells. *J. Phys. Chem. C* **2020**, *124*, 1872–1877. [CrossRef]